THE ROLE OF CASTING POROSITY IN FATIGUE PROPERTIES OF AL-SI 319 LOST FOAM CAST ALLOY

Yong-Bok Lee*, Aslak Siljander and Frederick V. Lawrence, Jr.****

(Received July 21, 1991)

The tensile, fracture toughness and fatigue properties of Al-Si 319 lost-foam-cast alloy were determined at room temperature. The fatigue properties of this alloy were also determined at 150℃. Fatigue cracks were always initiated at the largest casting pore. Initial pore sizes were measured using a scanning electron microscope. Surface replication showed that majority of the fatigue life was spent in fatigue crack propagation and permitted the estimation of the constants in the Paris power law and the threshold stress intensity factor (ΔK_{th}). The role of internal casting porosity was quantified using a linear elastic fracture mechanics (LEFM) model for fatigue crack growth. The predicted lives agreed with the measured values within a factor of two.

Key Words: Fatigue Properties, Surface Replication, Fatigue Life, Stress Intensity Factor, Casting Porosity

NOMENCLATURE

a : Crack depth (mm)
a_o : Initial crack depth (mm)
a_f : Final crack depth (mm)
a/c : Aspect ratio (dimensionless)
c : Half of the surface crack length (mm)
C : Crack growth coefficient (mm/cycle)
C^* : Correction factor (dimensionless)
C_1 : Correction factor (dimensionless)
C_2 : Correction factor (dimensionless)
C_3 : Correction factor (dimensionless)
C_4 : Correction factor (dimensionless)
da/dN : Crack growth rate (mm/cycle)
$g(\varphi)$: Correction factor (dimensionless)
$g(W)$: Correction factor (dimensionless)
K_{1max} : Maximum stress intensity factor (MPa$\sqrt{m}$)
K_{1min} : Minimum stress intensity factor (MPa$\sqrt{m}$)
ΔK_1 : Stress intensity factor range (MPa$\sqrt{m}$)
m : Crack growth exponent (dimensionless)
N : Number of cycles
N_f : Number of cycles to complete separation
Φ : Elliptical integral of the second kind
φ : Angle (rad)
R : Minimum-to-maximum stress ratio (dimensionless)
σ : Stress (MPa)
σ_{max} : Maximum stress (MPa)
σ_{min} : Minimum stress (MPa)
$\Delta\sigma$: Stress range (MPa)
σ_f : True fracture strength (MPa)
σ_{sn} : Sharp notch strength (MPa)
σ_u : Ultimate tensile strength (MPa)
σ_y : Tensile yield strength (MPa)
ε_f : True fracture ductility
Y_1 : Mode I geometry correction factor (dimensionless)

*Department of Mechanical Engineering, Hongik University, Sangsudong, Mapoku, Seoul 121-791, Korea
**Department of Materials Science and Engineering, University of Illinois at Urbana-Champaign, 208 North Romine Street, Urbana, Illinois 61801-2397, U.S.A.

1. INTRODUCTION

Preliminary uniaxial ($R=0.1$) fatigue data for the lost-foam-cast 319 aluminum alloy was developed by Reynolds Metal Company (Tyler, 1986). The Reynolds fatigue test specimens were small-sized and machined from the water jacket areas of Saturn engine blocks. The endurance limit of Al-Si 319 was estimated by Reynolds to be below 55 MPa.

The Reynolds project did not systematically study the effect of porosity (shringkage cavities) on the fatigue strength of this alloy. Consequently, the current program at the University of Illinois was initiated in September 1986. Baseline tensile and fatigue properties for the Al-Si 319 lost-foam-cast alloy tests were carried out using axial fatigue tests. The effects of both as-cast and machined surfaces on the fatigue resistance were determined as well as the influence of elevated temperatures 150℃. The role of internal casting porosity was quantified using a linear-elastic fracture mechanics (LEFM) model for fatigue crack growth.

2. EXPERIMENTAL PROCEDURES

2.1 Material Description

Specimens of Al-Si 319 lost-foam-cast alloy were cast and T5-heat-treated by the General Motors Corporation. The specimens were received as 16 mm diameter, 305 mm long bars. Specimens were machined to the final dimensions shown in Fig. 1. As-cast-gage-section samples were received ready to test ; thus, only the grip ends of these specimens were machined to the final dimensions shown in Fig. 1. The chemical composition and mechanical properties of this alloy are given respectively in Table 1 and Table 2.

2.2 Fatigue Tests

Fatigue tests for the lost-form-cast Al-Si 319 alloy were

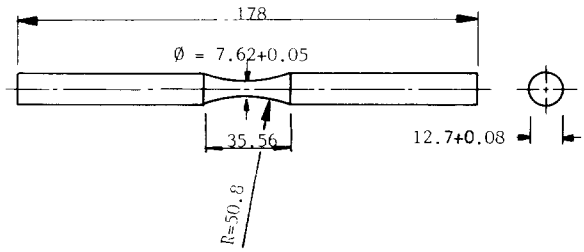

Fig. 1 Fatigue test specimen for room temperature and elevated temperature fatigue test (unit : mm)

Table 1 Chemical composition (%wt.) of Al-Si 319 alloy

Si	Cu	Mg	Fe	Ti	Zn	Mn	Pb	Sn	Ni	Cr
5.70	3.04	.75	.20	.08	<.1	.05	<.05	<.05	<.05	<.05

Table 2 Mechanical properties of Al-Si 319 lost foam cast alloy

Monotonic properties							Fracture toughness properties			
σ_y MPa	σ_u MPa	RA %	σ_f MPa	ε_f	HB	P_{max} KN	σ_{sn} MPa	σ_{sn} σ_y	K_{Ic} MPa	
228.1	228.1	0.26	237.8	0.0033	52	7.26	114.3	0.50	16.5	

performed using servo-hydraulic MTS fatigue test machines under load control with load ratio R=0.1 and at test frequency of 10 Hz. Failure was defined as complete separation of a specimen. Room temperature tests were performed in 99% relative humidity by surrounding the specimen gage section with a Tygon tube which water-saturated air was circulated. A schematic diagram of the test set-up is shown in Fig. 2. Elevated temperature tests were performed in air at 150℃. The specimens were heated by a Thermolyne heat tape which was wrapped around the gage section of the specimen. The gage section temperature was monitored at three locations using thermocouples.

2.3 Surface Crack Growth Observation

Replica experiments were performed on three specimens. The replica specimens had a uniform 25.4 mm gage section and were machined to the dimensions shown in Fig. 3. The replica specimens were polished after machining using aluminum oxide polishing tape together with Happich Simichrome polishing paste. This polishing eliminated machining marks from the specimen gage section surface. Tests were interrupted at regular intervals, approximately 10% of the expected life and acetyl cellulose replicas (Bioden R.F.A 0.034 mm thick) were taken of whole specimen gage section surface. The replica tape was softened with Methyl acetate solution (Kodak 520) and allowed to dry on the specimen. Once imprinted with the surface topography, the replicas were stripped, placed between glass slides, and later examined using transmitted light optical microscopy. Details of the replicating procedure can be found in Refs. (Fash,1980, 1983, Waill, Weinacht, Bannantine, 1986).

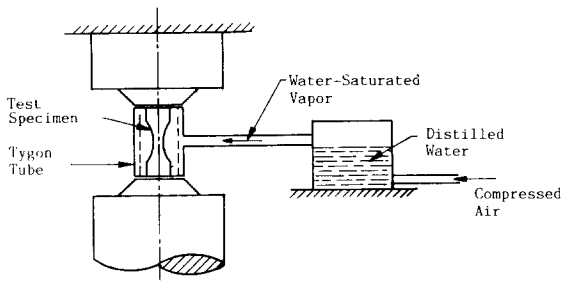

Fig. 2 Schematic of the room temperature test set-up

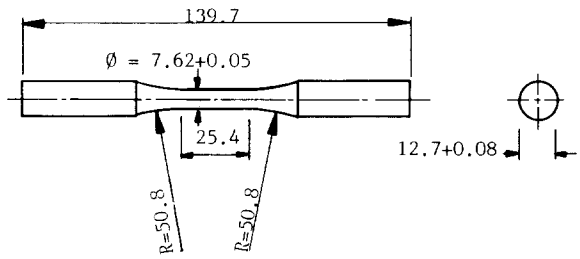

Fig. 3 Fatigue test specimen for surface replication studies (unit : mm)

2.4 Fractography

Scanning electron microscope (SEM) examination of the fracture surfaces showed extensive internal porosity in the majority of the specimens and proved that porosity was the major cause of fatigue crack initiation and subsequent growth. The largest shrinkage cavity size found was approximately 2 mm in diameter. Example of typical fatigue crack initiating casting porosity is shown in Fig. 4.

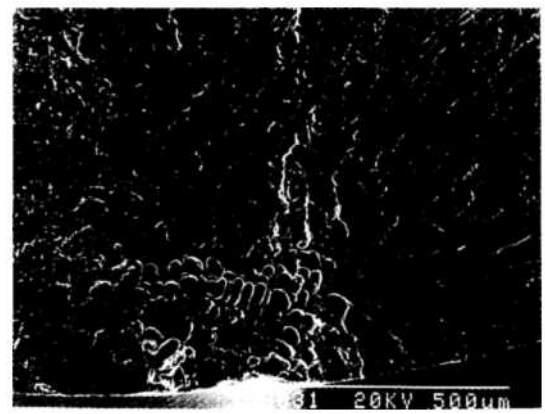

Fig. 4 Initiating pore at the surface of as-cast specimen T3-318 (100x)

3. RESULTS AND DISCUSSION

3.1 Axial Fatigue Test Results

The fatigue test results are given in Figs. 5~8. Test temperatures and surface finish seemed to have no significant effect on the fatigue strength of this alloy. Rather, as will be shown, the large scatter in the test results was determined by the size of the largest casting pore. Some failures initiated in the grip-end sections of the specimens, where the stresses were nominally 36% of the stresses in the gage section.

Approximately five of the 50 specimens tested failed in the grip section. It is questionable whether the stresses in these grip section locations are accurately known since many of the gage section initiation sites are within one diameter of the grips and the large surface shear stresses applied by the grips. The grip section data are therefore distinguished from gage section failures by being plotted as solid symbols in all plots, and the low values for these data are suspect. These grip section failures do indicate that fatigue cracks do not necessarily originate in the regions of the highest nominal stresses but it often in lower stress locations where the largest defect is located. More exactly, fatigue failure should initiate at the location having the highest initial value of stress intensity factor, that is, the maximum value of the product of pore size and the nominal local stress in the pore's vicinity.

3.2 Observations of Surface Cracking Behavior

Fatigue cracks could be traced back to their initiation sites in the replica studies and the initiation sites were inevitably at the edge of a shrinkage cavity of the specimen surface. In general, these cavities were surface notches and were characteristic of this alloy and casting process. These statements were also generally true for the as-cast specimens, but the surface roughness of the as-cast surface provided the critical notch in one or two cases whithout the involvement of a large pore : see Table 3.

Cracks were initiated very early in life, that is during the first 5 to 10% of the total fatigue life. Thus, the majority of the fatigue life (90~95% of total life) was spent in propagating and linking cracks(Suh, Kitakawa and Yuuki, 1983). In all cases, cracks were observed to propagate perpendicular to the maximum principal stress, i.e., Forsyth Stage Ⅱ cracks (Forsyth, 1961).

A computer program was written to estimate the stress intensity factor(SIF) for a semi-elliptical edge crack in a cylindrical specimen. Crack depths were calculated based on the assumption of a fixed aspect ratio : see Fig. 9. Values for the surface half crack length, c were extracted from acetate replicas. Crack depth, a was measured on several fractured test specimens, and these results showed that the aspect ratio (a/c) was approximately 0.95, i.e., nearly semi-circular.

Fatigue crack gorwth rate was measured using information from the replicated specimens. A plot of crack depth versus number of cycles was obtained by tracing the dominant crack back through the set of replicas and measuring its tip-to-tip length : see Fig. 10. When two or more cracks were well developed and near linking, the sum of their lengths was considered as the crack length at the particular life. An averaging exponential best fit was applied to the crack depth versus number of cycles data (Fig. 10) in order to avoid difficulties with sudden jumps in crack depth due to the linking of cracks. Thus, the results indicate the average crack growth.

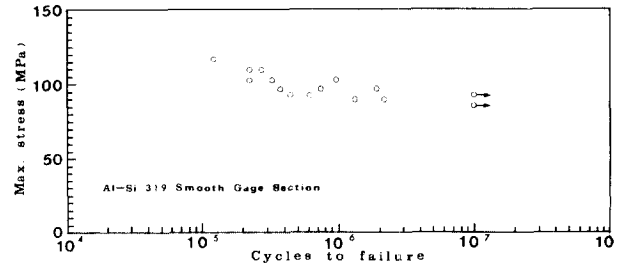

Fig. 5 Fatigue test results for Al-Si 319 : 12 micron finish, 99% relative humidity, room temperature. R=0.1, f=10 Hz.

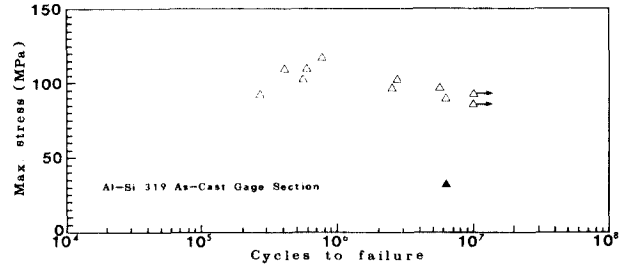

Fig. 6 Fatigue test results for Al-Si 319 : as-cast surface, room temperature, R =0.1, f =10 Hz. Solid symbols denote grip section failures

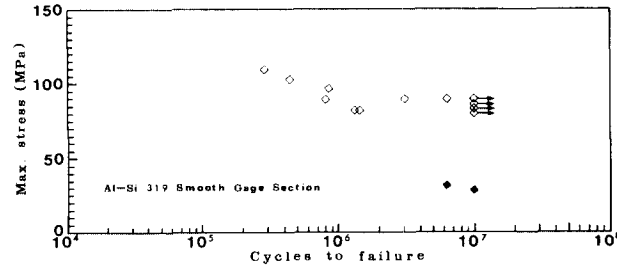

Fig. 7 Fatigue test results for Al-Si 319 : 12 micron finish, 150℃ temperature, R=0.1, f=10 Hz. Solid symbols denote grip section failures

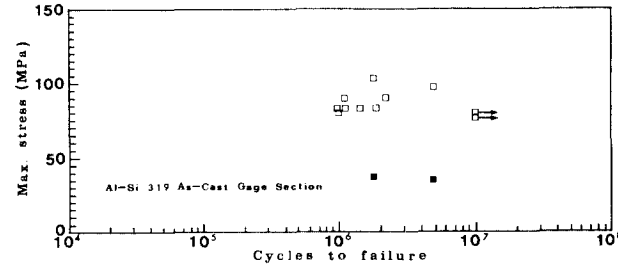

Fig. 8 Fatigue test results for Al-Si 319 : as-cast surface, 150℃ temperature, R =0.1, f =10 Hz. Solid symbols denote grip section failures

The average crack grwoth rate, da/dN, was calculated by using the seven point polynomial method. Crack growth was assumed to follow the exponential best fit expression. By knowing the crack growth rate and the corresponding crack depth the standard da/dN versus the maximum SIF plot shown in Fig. 11 could be developed (over a limited range of growth rates). From this limited information, the constants in

Table 3 Comparison of the actual test results with the analytical fatigue life predictions

Specimen ID	Temp. (°C)	Gage section	σ_{max} (MPa)	a (mm)	N (actual)	Np (predicted)
T1-2	150	as-cast	83	0.32	1,413,300	3,223,000
T1-10**	150	smooth	28.8	0.86	9,944,800	32,465,000
T1-14	150	smooth	90	0.82	807,300	1,119,000
T1-13	150	etched	83	***	967,700	
T1-18**	150	smooth	32.4	1.11	6,315,500	16,922,000
T2-22	R.T.	smooth	103	0.73	972,000	840,000
T2-26	R.T	as-cast	103	0.6	560,270	1,011,000
T2-21	R.T	as-cast	90	0.2*	6,279,900	3,522,000
T2-23	150	smooth	90	0.33	3,097,000	2,471,000
T2-28	R.T.	smooth	93	0.9	617,430	918,000
T2-101	150	as-cast	90	0.5	1,084,000	1,777,000
T2-20	R.T.	as-cast	93	2.1	268,600	217,000
T2-20	R.T.	smooth	97	0.63	1,917,300	1,157,000
T2-13	R.T.	smooth	97	0.77	747,700	954,000
T3-322	R.T.	smooth	110	1.45	222,610	294,000
T3-311	R.T.	smooth	93	1.20	443,090	646,000
T3-315	R.T.	smooth	117	0.95	121,010	434,000
T3-315	R.T.	as-cast	110	0.78	592,410	645,000
T3-318	R.T.	as-cast	97	0.45	2,514,540	1,549,000
T3-313	R.T.	as-cast	117	0.35	769,240	1,076,000
T3-312	R.T.	as-cast	103	0.25	2,748,310	2,015,000
T3-314	R.T.	smooth	110	0.72	272,660	699,000
T3-317	R.T.	as-cast	97	0.83	5,671,410	882,000
T3-323(R)	R.T.	smooth	103	1.11	222,081	527,000

* : Failure at pore and cast surface roughness triple point
** : Grip end failure
*** : No pore evident, failure originated at cast surface roughness triple point
R : Replicated specimen

the Paris equation were estimated : $C=2.05\times10^{-8}$ and $m=3.12$. These data agree reasonably well with da/dN vs ΔK data for 7075 and 2024 wrought alloys : see Fig. 12(Campbell, Gerberich and Underwood, 1982).

3.3 Fatigue Life Prediction Based on the LEFM Model

The fatigue crack propagation life can be estimated from the Paris equation

$$da/dn=C(\Delta K_I)^m=C(K_{Imax}-K_{Imin})^m \quad (1)$$

In all of the tests conducted, the minimum-to-maximum stress ratio was kept constant, i.e.

$$R=K_{Imin}/K_{Imax}=\sigma_{min}/\sigma_{max}=0.1 \quad (2)$$

Thus

$$\Delta K_I=0.9K_{Imax} \quad (3)$$

and

$$K_I=Y_I\sigma\sqrt{\pi a}\ [Y_I=C^*/\Phi] \quad (4)$$

Where

$$C^*=\left\{C_1+C_2\left(\frac{a}{B}\right)^2+C_3\left(\frac{a}{B}\right)^4\right\}C_4 g(\varphi)\,g(W) \quad (5)$$

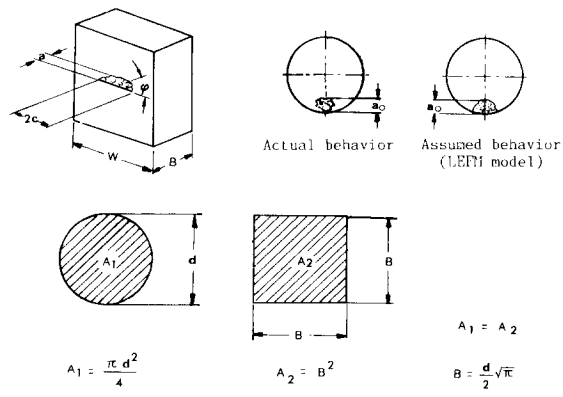

Fig. 9 Fracture mechanics modelling of surface shrinkage pore. An equivalent rectangular specimen shape was assumed

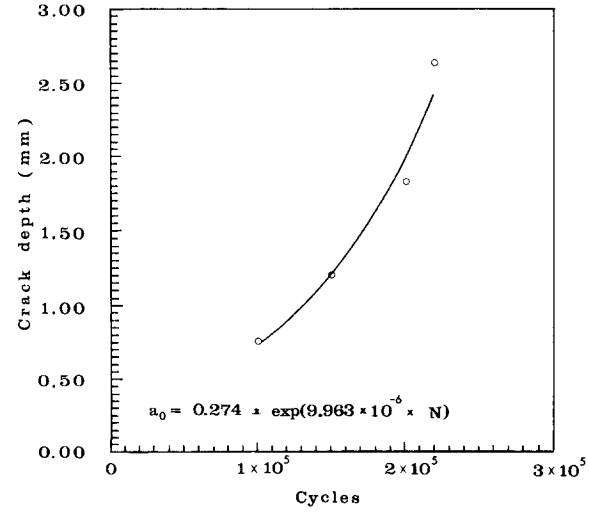

Fig. 10 Crack depth versus cycles. Measurements take for surface replicas. An exponential fit to the data is shown. Data at short crack lengths was no used due to uncertainty as to the stress intensity factor model near a shrinkage cavity

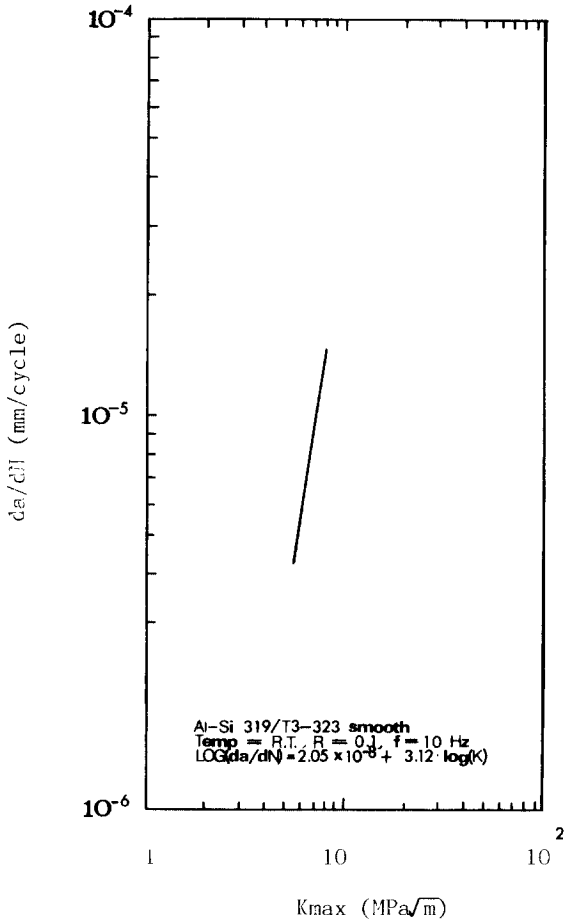

Fig. 11 Crack growth rate vs. maximum stress intensity factor. Data is extrapolated to a growth rate of 10^{-6} mm/cycles to estimate $\Delta K_{th}=3.5$ MKPa$\sqrt{m}$

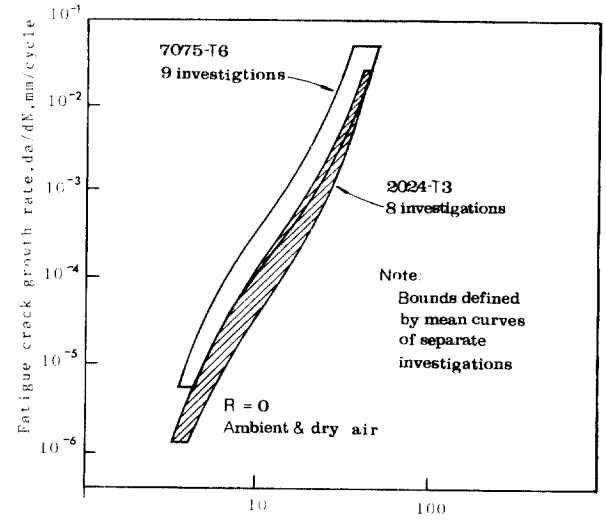

Fig. 12 Fatigue crack growth behavior reported for 7075 and 2024 aluminum alloy from Campbell, Gerberich and Underwood, 1982

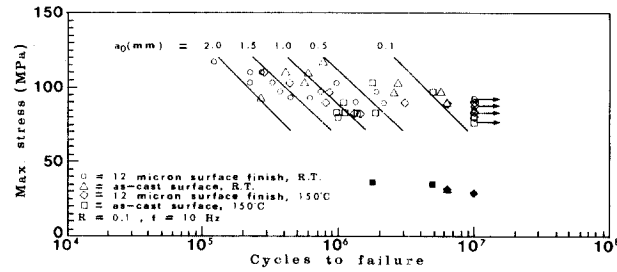

Fig. 13 All fatigue test data for lost foam cast Al-Si 319. solid symbols denote grip section failures. Solid lines indicated predicted S-N diagrams for the indicated initial surface pore size.

$$C_1=1.13-0.09\left(\frac{a}{c}\right) \tag{6}$$

$$C_2=-0.54+\frac{0.89}{0.2+\left(\frac{a}{c}\right)} \tag{7}$$

$$C_3=0.5-\frac{1.0}{0.65+\left(\frac{a}{c}\right)}+14\left\{1.0-\left(\frac{a}{c}\right)\right\}^{24} \tag{8}$$

$$C_4=1+\left\{0.1+0.35\left(\frac{a}{B}\right)^2\right\}(1-\sin\varphi)^2 \tag{9}$$

$$g(\varphi)=\left\{\sin^2\varphi+\left(\frac{a}{c}\right)^2\cos^2\varphi\right\}^{\frac{1}{4}} \tag{10}$$

$$g(W)=\left\{\sec\frac{\pi c}{W}\left(\frac{a}{B}\right)^{\frac{1}{2}}\right\}^{\frac{1}{2}} \tag{11}$$

$$\Phi=\int_0^{\frac{\pi}{2}}\left\{1-\left(\frac{c^2-a^2}{c^2}\right)\sin^2\varphi\right\}^{\frac{1}{2}}d\varphi \tag{12}$$

The function C^* is the boundary-correction factor for tension (Newman and Raju, 1981).

The mode I geometry correction factor Y_1 has been (Hua, 1984) to be almost constant for aspect ratios of 0.5 to 1.0. Thus

$$\int_0^N dN=\int_{a_f}^{a_0}\frac{da}{C(0.9\,Y_I\sigma_{max}\sqrt{\pi a})^m} \tag{13}$$

$$N_p=\frac{{a_f}^{1-m/2}-{a_0}^{1-m/2}}{C(0.9\,Y_I\sigma_{max}\sqrt{\pi})^m} \tag{14}$$

Fatigue crack propagation life (N_p) was thus predicted for various assumed initial semi-circular surface crack depths simulating the shrinkage cavity depth on the specimen surface. These predicted "S-N curve" by LEFM were superimposed on the uniaxial, constant amplitude fatigue test results, see Fig.13.

3.4 Comparison of Predicted and Observed Fatigue Lives

The actual test results are compared with the predicted fatigue life in Table 3. This comparison is based on the post-failure SEM measurements of the actual initiation pore depths. The pore depths were measured along the surface normal into the material to the deepest pore-matrix interface and were approximated as a semi-circular defect even though these pores were often quite irregular in shape. The actual versus predicted fatigue life results in Table 3 are displayed graphically in Fig. 14, where all of the displayed data points have been measured with respect to the pore size. Most of the predicted lives agree quite well with the actual lives within a factor of two.

It should be noted that the crack growth constants C and m in the Paris equation determined in this study are for R=0.1 constant amplitude, sinusoidal loading. However, field measurements conducted by General Motors Corporation have recently shown that the stress ratio (R) is closer to 0.9 than 0.

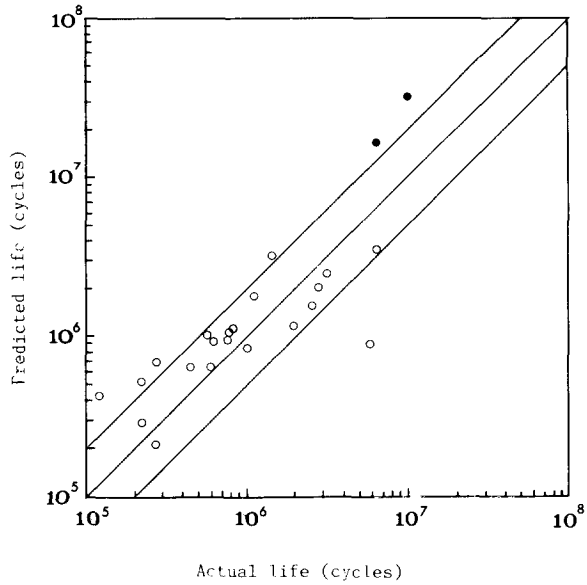

Fig. 14 Comparison of the actual and predicted fatigue lives of the specimens for which the initiation pore size was measured by SEM fractograghy. Solid symbols indicate grip section failures

1 as was assumed in this study. If crack closure plays an important role in determining the fatigue crack growth rates of this alloy, the crack growth rates for real components in-service could be somewhat higher resulting in shorter lives. Additional tests are suggested to check the stress ratio(R) dependence of this alloy.

3.5 Fatigue Limit Based on the Threshold Stress Intensity factor

If the threshold SIF for long cracks were known, it would mean that physically long cracks would not propagate below this threshold value. In other words, by knowing the maximum threshold SIF and also the initial depth of the semi-circular surface flaw the stress corresponding to the fatigue limit, a safe design stress, could be calculated. From Eq. (5)

$$\Delta\sigma_{th}=\frac{\Delta K_{th}}{Y_I\sqrt{\pi a_{th}}} \tag{9}$$

The threshold SIF (ΔK_{th}) can be roughly estimated from the crack growth data in Fig. 11. to be about 3.5 MPa$\sqrt{m}$. Similar estimates of ΔK_{th} can be obtained from the data for 7075 and 2024 wrought alloy in Fig. 12. Thus, by solving Eq. (14), the fatigue limit for different, initial, semi-elliptical surface flaws can be evaluated. While there is still not a great deal of evidence to firmly assert it, it appears that the safe design stress depends upon the size of the maximum casting pore. If pores as large as 2 mm are unavoidable and if (ΔK_{th}) is about 3.5 MPa$\sqrt{m}$ as it appears to be, then design stresses no large than 60 MPa would seem permissible. If the maximum pore size is l imited to 1mm then the permissible maximum design stress would be 87 MPa. The safe design stress to avoid fatigue is therefore nearly completely dependent on the size of the largest casting pore.

As seen in Fig. 15, the Reynolds data results lie within, although at the bottom of, the scatter band of the current results. Thus if it develops that the Rynolds specimens generally contained large pore on the order of 2 mm, there is no

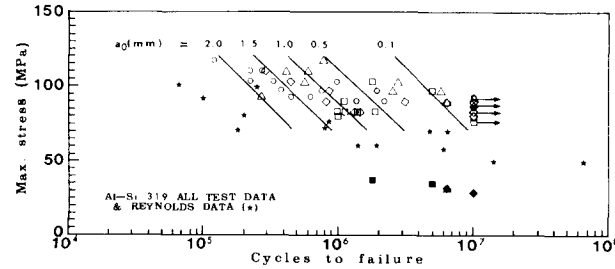

Fig. 15 Summary of all fatigue test data and Reynolds data for Al-Si 319 lost foam cast material and the predicted S-N diagrams

apparent inconsistency between the Reynolds results and ours. The initiating pore sizes of the Reynolds specimens should be remeasured.

The importance of the value of the threshold stress intensity factor is such that additional experiments should be performed. One idea is to lost foam cast compact tension specimens of the 319 Al-Si alloy to determine ΔK_{th} and K_{Ic} directly in a standard test.

Finally, it should be noted that components (engine blocks) in service experience stress histories that are seldom constant amplitude. A limited program of variable amlplitude fatigue testing could be consdiered.

4. CONCLUSIONS

(1) The surface finish of the samples had only a small effect on the fatigue characteristics of the 319 Al-Si alloy.

(2) The testing temperature had only a small effect in the fatigue behavior of the 319 Al-Si alloy.

(3) The shrinkage cavities played a major role in the fatigue behavior of lost foam cast Al-Si alloy. These defects were due to the casting process, and they provided very irregular initial near surface flaws.

(4) The replica studies showed that fatigue cracks initiated either from the multiple casting pores or from the surface texture triple points or from the combination of the two. These flaws then grew perpendicular to the fluctuating tensile principal stress. The majority of the fatigue life was spent in propagating and linking fatigue cracks. The location of the largest pore always dictated the fatigue crack initiation site.

(5) By treating the irregular-shaped surface flaws as semi-elliptical surface flaws, a fatigue crack growth model was developed which predicted the fatigue lives of the lost foam cast Al-Si 319 alloy spcimens within a factor of two.

REFERENCES

Bannantine, J.A., 1986, "observations of Tension and Torsion Fatigue Cracking Behavior and the Effect of Multiaxial Damage Correlations," Division Report No. 128, Department of Mechanical and Industrial Engineering, University of Illinolis at Urbana-Champaign, Urbana, Illinois.

Campbell, J. E., Gerberich, W.W. and Underwood, J.H., 1982, "Application of Fracture Mechanics for selection of Metallic Structural Materials," ASM.

Fash, J., 1980, "Fatigue Crack Initiation and Growth in Gray Cast Iron," FCP Report No.35, College of Engineering,

University of Illinois at Urbana-Champaign, Urbana, Illinois.

Fash, J., 1983, "An Evaluation of Damage Development During Multiaxial Fatigue of Smooth and Notched Specimens," Materials and Design Division Report No. 123, Department of Mechanical and Industrial Engineering, University of Illinois at Urbana-Champaign, Urbana, Illinois.

Forsyth, P.J.E., 1961, "A Two-Stage Process of Fatigue Crack Growth," Proc., Crack Propagation Symposium, Cranfield, pp. 76~94.

Newman, Jr. J. C. and Raju, I.S., 1981, "An Empirical Stress-Intensity Factor Equation for the Surface Crack," Engineering Fracture Mechanics, Vol.15, No.1-2, pp. 185~192.

Hua, C.T., 1984, "Fatigue Damage and Small Crack Growth During Biaxial Loading", Report No. 109, Department of Mechanical and Industrial Engineering, University of Illinois at U-C, urbana, Illinois.

Suh, C.M., Kitakawa, H. and Yuuki, R., 1983, "Basic Characteristics of Micro-Fatigue-Cracks on the Unnotched Smooth Specimens," KSME, W7-1, pp. 28~35.

Tyler, G.B., 1986, "Axial Fatiue Testing of Lost Foam 319 and 390 Alloys," Reynolds Metals Company project No.4R-4C3-Z458S, Product and Process Development Laboratory/ Chemical, Mechanical and Casting Technology Department.

Waill, L., 1986, "Crack Obsevations in Biaxial Fatigue," Material and Design Division Report No. 108, Department of Mechanical and Industrial Engineering, University of Illinois at Urbana-Champaign, Urbana, Illinois.

Weinacht, J., 1986, "Fatigue Behavior of Gray Cast Iron Under Torsional Loads", Materials and Design Division Report No. 126, Department of Mechanical and Industrial Engineering, University of Illinois at Urbana-Champaign, Urbana, Illinois.